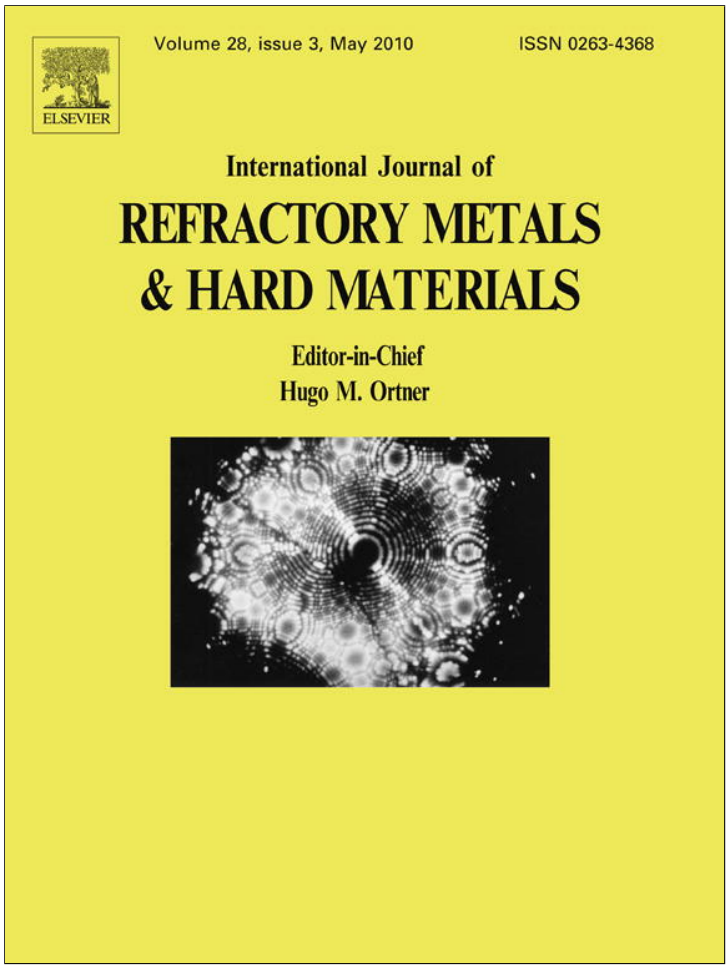

Int. Journal of Refractory Metals & Hard Materials 28 (2010) 399–406

Contents lists available at ScienceDirect

Int. Journal of Refractory Metals & Hard Materials

journal homepage: www.elsevier.com/locate/IJRMHM

Sinter and hot isostatic pressing (HIP) of multi-wall carbon nanotubes (MWCNTs) reinforced ZTA nanocomposite: Microstructure and fracture toughness

J. Echeberria [a], J. Ollo [a], M.H. Bocanegra-Bernal [b,*], A. Garcia-Reyes [c], C. Domínguez-Rios [b], A. Aguilar-Elguezabal [b], A. Reyes-Rojas [b]

[a] CEIT and TECNUN (University of Navarra), 20018 San Sebastian, Spain
[b] Centro de Investigación en Materiales Avanzados, CIMAV S.C., Laboratorio Nacional de Nanotecnologia, Miguel de Cervantes # 120, Complejo Industrial Chihuahua, Chihuahua 31109, Mexico
[c] Interceramic, Departamento de Investigación y Desarrollo, Av. Carlos Pacheco 7200, Chihuahua 31060, Mexico

ARTICLE INFO

Article history:
Received 13 October 2009
Accepted 18 December 2009

Keywords:
Zirconia toughened alumina
Crack deflection
Hardness
Fracture toughness
Pull-out

ABSTRACT

This work describes the microstructure and fracture toughness of zirconia toughened alumina (ZTA) nanocomposite in which multi-wall carbon nanotubes (MWCNTs) and nanosized ZrO_2 particles were used as reinforcement. The ZTA nanocomposites with additions of 0, 0.005, and 0.01 wt.% MWCNTs and 2 wt.% nanosized ZrO_2 particles were pressureless sintered in an anti-oxidant sagger with graphite powder bed at 1520 °C during 1 h in air and then HIPed at 1475 °C in argon atmosphere 1 h at a pressure of 150 MPa. Relative densities ranging 94–98% were reached. In HIPed composites the hardness and fracture toughness values were increased up to ~17% and ~37%, respectively, compared to the "as sintered" composites free of carbon nanotubes. A combined fracture mode, crack deflection, pull-outs of a small amount of carbon nanotubes, and bridging effect were the mechanisms leading to the improvement in fracture toughness.

1. Introduction

From many years, there has been an increasing interest in development of advanced ceramic composites with excellent mechanical and physical properties by incorporating strong particles/whiskers into ceramic matrices [1–3]. Since carbon nanotubes were first observed by Iijima [4], the potential for nanoreinforced ceramics with single-wall and multi-wall carbon nanotubes (SWCNT and MWCNT), having extraordinary stiffness and strength, represents an important step in the development of ceramic nanocomposites with improved fracture toughness and strength over monolithic ceramic materials [5,6]. Carbon nanotubes (generally abridged as CNTs) have exceptional mechanical properties where their tensile strength and Young's modulus have been measured to be as high as 200 GPa and 1 TPa, respectively, even much higher than that of whiskers [1,7,8]. Yu et al. [9] measured Young's modulus of the outermost layer on MWCNTs as varying from 270 to 950 GPa and the tensile strength of this layer as ranging from 11 to 63 GPa.

There are two main types of carbon nanotubes: single-wall carbon nanotubes (SWCNT) consisting of a single graphene sheet rolled-up into a cylinder with diameters as small as 1 nm [10,11]. Otherwise, multi-wall carbon nanotubes (MWCNTs) are simply composed of a number of concentric single-walled nanotubes held together with relatively weak van der Waals forces [5,12] where the measured interlayer distance (0.34 nm) is very close to that measured between graphene sheets in graphite. Nanotubes are long, slender fullerenes where the walls of the tubes are hexagonal carbon (graphite structure) and often capped at each end [5].

In order to prepare single-walled and multi-walled nanotubes methods that include arc discharge in the absence or presence of metal, laser-vaporization of a metal–graphite composite target [12,13] or spray pyrolysis [14] are frequently used. Considering the application of carbon nanotubes as reinforcement in ceramic composites which requires an economic production of CNTs, gas phase techniques like chemical vapor deposition (CVD) can offers great potential for optimization of nanotube production and also allows to synthesize aligned arrays of carbon nanotubes with controlled diameter and length. It is noteworthy that although single-walled nanotubes possess better properties compared with multi-walled ones, their production and purification is easier and therefore, makes it more economical for most applications including dispersing in ceramic matrix [13].

A lot of research work on carbon nanotubes contained composites has concentrated on polymer-matrix materials for improved electric conductivity, optical devices and higher strength [15]. However, there are few studies carried out on CNTs reinforced

* Corresponding author.
E-mail address: miguel.bocanegra@cimav.edu.mx (M.H. Bocanegra-Bernal).

0263-4368/$ - see front matter © 2009 Elsevier Ltd. All rights reserved.
doi:10.1016/j.ijrmhm.2009.12.007

ceramic matrix composites, and successful cases are even fewer [16]. It is well known that CNTs tend to be agglomerated each other due to strong van der Waals attractive forces and their fibriform structure, particularly when the matrix material is in the granular form such as ceramic powders, resulting in the degradation of the mechanical and physical of the composite [17,18]. The major concern is to obtain a uniform dispersion of nanotubes in the matrix. Single-wall as well as multi-wall carbon nanotubes and different processing techniques have been used in order to prepare CNTs/ceramic nanocomposites including sinter and post-hot isostatic pressing (HIP) to attain full densification [2,19], and hot pressing (HP) [20]. However, it is noteworthy that consolidation by means of hot pressing at temperatures higher than 1500 °C damages some CNT producing disordered grapheme layers which gather at matrix junctions [10]. Recently spark plasma sintering (SPS) has been used with the aim to reduce the damage of the carbon nanotubes by the use of low sintering temperatures and short sintering times [2,21].

The use of the extraordinary mechanical properties of carbon nanotubes as reinforcement in ceramics has not been very successful although some interesting achievements have been obtained. For example, An et al. [22] studied the influence of CNT content on the tribological properties of CNT/Al_2O_3 composites and reported an increase in microhardness of 30% more than pure Al_2O_3; Siegel et al. [23] obtained an increase in fracture toughness about 24% in alumina reinforced with 10 vol.% MWCNTs. More recently, Zhan et al. [24] reported a fracture toughness of 9.7 MPa $m^{1/2}$ in spark plasma sintered 10 vol.% SWCN–Al_2O_3 nanocomposite at 1150 °C during 3 min being nearly three times that of nanocrystalline alumina. It is well known the ZrO_2 additions may increase the fracture toughness of ceramic materials due to the tetragonal to monoclinic phase transformation accompanied of a volume increasing generating stresses in the ceramic matrix, which results into difficult crack propagation [25]. In reason of this, in this work, we report for the first time the microstructure, hardness and fracture toughness before and after HIP of a new ceramic nanocomposite based Al_2O_3 (zirconia toughened alumina (ZTA)) reinforced by MWCNTs and pure monoclinic and nanosized ZrO_2 particles. The excellent mechanical and chemical properties of multi-wall carbon nanotubes could offer the opportunity for advances in design of multipurpose orthopedic implants, taking also advantage that they are highly hydrophobic, chemically inert, as well as little soluble in both organic and aqueous solvents. However, assessments of the *in vitro* and *in vivo* pharmaceutical profile of the carbon nanotubes are necessary before these can be considered for future clinical applications [26].

2. Experimental procedure

High purity α-Al_2O_3 (Baikalox SM8, Baikowski, USA; primary particle size 50 nm, purity >99.99%, surface area 10 $m^2\,g^{-1}$), MgO (500A, UBE Chemical Industries, Japan; primary particle size 53 nm, purity >99.999%, surface area 32 $m^2\,g^{-1}$), ZrO_2 + 3 mol% Y_2O_3 (thereafter abridged as TZ-3Y, Tosoh, Japan; primary particle size 75 nm, purity >99.99%, surface area 17 $m^2\,g^{-1}$), monoclinic ZrO_2 (Aldrich, USA; primary particle size <50 nm, purity >99.99%, surface area 15–35 $m^2\,g^{-1}$) powders and MWCNT (Catalysis Laboratory of CIMAV S.C. according to process detailed in Ref. [14], diameter 70–110 nm, length 120–160 μm, purity >95%, surface area 25 $m^2\,g^{-1}$) were used as starting materials. An homogeneous mixture of Al_2O_3 + 0.025% MgO + 13% TZ-3Y + 2% $ZrO_{2(m)}$ with additions of 0.005 and 0.01 wt.% of MWCNTs was prepared. A composite without additions of carbon nanotubes was also prepared as comparison. Care was taken to mix the nanopowders and MWCNTs. The as-received multi-wall carbon nanotubes were carefully dispersed in 500 mL ethanol with ultrasonic agitation for 2 h. Nanopowders were intensely mixed with the dispersed carbon nanotubes alcohol media by stirring with a magnetic stir bar until most of ethanol was evaporated and then the mixture was dried at 100 °C for 12 h. The agglomerated mixture was ground intense and carefully in an agate mortar. To avoid any variations that could occur due to relative ambient humidity changes, all experiments were done at the same time.

About 2.5 g of the mixture was uniaxially pressed at 50 MPa in a disk (steel die) with 16 mm diameter and 7 mm height using an Elvec Hydraulic Press (by ELVEC S.A. de C.V., Mexico) at a constant strain rate. As shown in Fig. 1 (for pressureless sintering experiments), green samples with additions of carbon nanotubes were placed into an alumina sagger with high purity graphite packing powder (graphite powder, crystalline, −300 mesh, 99%, Alfa Aesar), where the alumina powder fills the space between the two high alumina crucibles. A third crucible covers the one containing the graphite powder bed with the sample. Samples without additions of MWCNT were set in Al_2O_3 crucible with a ZrO_2 + Al_2O_3 powder bed. All samples were sintered at 1520 °C during 1 h in air at a heating rate of 10 °C m^{-1}. After sintering, the furnace was shut off and it was allowed to cool down. For hot isostatic pressing experiments a set of sintered samples with and without additions of MWCNTs was introduced in a boron nitride crucible with an alumina powder bed to minimize possible reaction with the graphite heating element and subsequently hot isostatic pressed in an ASEA–HIP (QIH-6) equipment (by ABB, Kent, WA, USA) at 1475 °C at heating rate of 20 °C min^{-1} under argon atmosphere at a pressure of 150 MPa during 1 h. Density was measured geometrically and by a Quantachrome Multipycnometer (by Quantachrome Instruments, USA) using helium as displacement gas for the as-sintered and HIPed samples.

The samples were ground through by SiC paper in sequence of #400, #800, and #1200, and then polished by diamond pastes of both 0.5 and 0.25 μm. Samples without CNTs additions were thermally etched in air at 1370 °C for 45 min, while the samples with carbon nanotubes additions followed the same procedure but using the set shown in Fig. 1 in order to preserve the carbon nanotubes. The polished and fracture surfaces as well as the MWCNTs were characterized by scanning electron microscopy (SEM: JEOL JSM 5800 LV, Japan, and FEG SEM: JEOL JMS 7000F, Tokyo, Japan) using an accelerating voltage of 2–10 kV. Transmission electron microscopy (TEM: CM200 Phillips, the Netherlands) was applied to observe the morphology of the carbon nanotubes. The average grain size in as-sintered and HIPed composites was measured using the linear intercept technique using 300–400 grains for each sample.

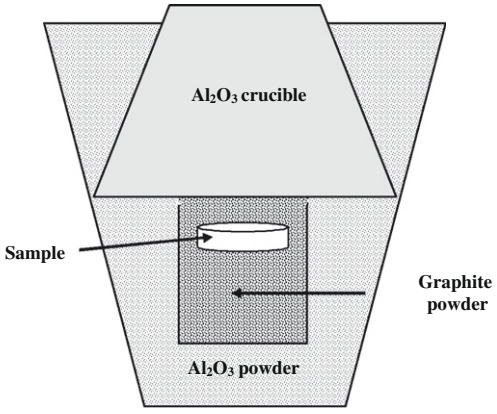

Fig. 1. Schematic showing sagger structure to pressureless sintering of ZTA composites in air.

Vickers hardness measurements were carried out on sintered samples by using a microhardness tester FM-7 (by Future-Tech, Tokyo, Japan). Indentations were made on polished surfaces with a load of 1 kg held for 10 s. Approximately 20–30 indents were made for each composition and the average hardness was determined. The corresponding indentations sizes and crack lengths were measured using an optical microscope Olympus PMG3 (by Olympus Co., Japan). The indentation fracture toughness (K_{IC}) was derived from the average crack length. For a ratio $c/a > 2.5$ (present study), where c is the crack length and a is the half diagonal length of the indentation impression, K_{IC} is calculated using the following equation [27]:

$$K_{IC} = 0.0752P/c^{3/2} \quad (1)$$

where K_{IC} is the fracture toughness, P the load and c the crack length.

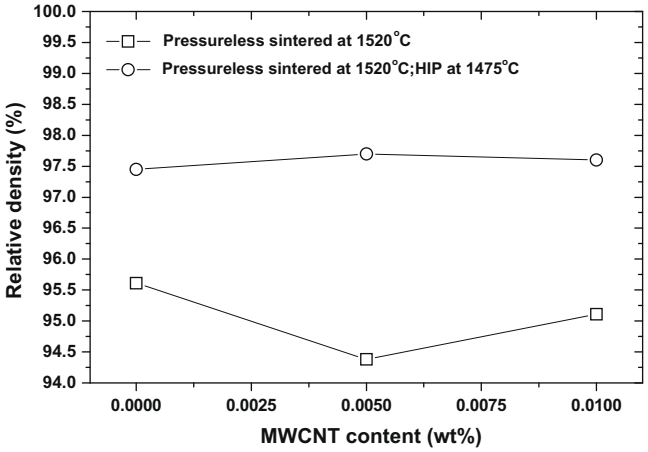

Fig. 3. Relative density as a function of the MWCNT content.

3. Results and discussion

SEM and TEM images of the starting multi-wall carbon nanotubes are shown in Fig. 2. Numerous carbon nanotubes (Fig. 2a) having similar diameters (approximately 65 nm) with a length ranging from several hundred of nanometers, appearing to be very flexible, are observed. The Fig. 2b is a typical TEM micrograph showing two MWCNTs with walls aligned corresponding to the final step of the formation mechanism of multi-wall carbon nanotubes. This micrograph clearly shows that the nanotubes are multi-walled hollow tubes and not solid fibers. Impurities in the form of catalyst particles as well as amorphous carbon can also be observed.

The MWCNTs reinforced ZTA composites were sintered at 1520 °C and subsequently HIPed at 1475 °C under argon atmosphere. The relative densities of the specimens as a function of the carbon nanotubes content are shown in Fig. 3. It can be noted that the relative densities of the composites before and after HIP are in all cases higher than 94%. For the as-sintered samples, the density for composite with 0.005 wt.% carbon nanotubes addition was slightly lower suggesting a connected porosity with the clusters of the CNTs present in the microstructure which hinders the densification in the specimens due to the formation of agglomerates. Increasing the CNTs content up to 0.01 wt.% the relative density is slightly increased, but it is still lower than that of the composite without CNTs. This observation is in contrast to the general trend which is agreement with observations of Ahmad and Pan [28] and Sun et al. [15] for alumina reinforced with different amounts of MWCNTs, where the relative density is slightly decreased when the CNTs content is increased. It is also observed in this figure that the density of the pressureless sintered samples is increased by HIP (carried out at a lower temperature than PS: 1475 vs. 1520 °C), indicating that in all cases closed porosity was obtained by pressureless sintering, that can be almost all removed by hot isostatic pressing. Besides, the relative density of the HIPed specimens is almost constant for the different CNTs contents. In fact, these density data clearly showed that, within experimental scatter, the sintered densities before and after HIP treatment are approximately the same. It is also shown that the maximum density obtained after sintering (by HIP) was approximately 98% TD.

X-ray diffraction (XRD) studies not shown here in 0.005 and 0.01 wt.% multi-wall carbon nanotubes reinforced zirconia toughened alumina nanocomposites, revealed that the composites consisted of mainly Al_2O_3 phase, t-ZrO_2 phase and small amounts of m and c-ZrO_2 phases. Fig. 4 shows representative SEM micrographs of polished and thermally etched surfaces of as-sintered specimens with (Fig. 4a) and without (Fig. 4b) additions of MWCNTs, respectively. On the other hand, pressureless sintered and HIPed zirconia toughened alumina (ZTA) composites with 0.01 wt.% carbon nanotubes content is shown in Fig. 4c. As can be seen in these figures, all composites exhibited a similar microstructure with measured grain sizes of 0.6 ± 0.2, 0.60 ± 0.26 and 0.7 ± 0.3 μm for pressureless sintered composites with 0 wt.%, 0.01 wt.% MWCNTs content and HIPed samples reinforced with 0.01 wt.% MWCNT, respectively. In these figures ZrO_2 grains are also observed (the brightest phase) homogeneously distributed in an Al_2O_3 matrix (darker phase). The presence of zirconia particles on the grain boundaries suggests that they could inhibit notably the alumina grain growth. Likewise, it is clearly observed that all samples were crack-free with submicron equiaxed grains and some isolated pores only in the case of pressureless sintered ZTA (Fig. 4a and b). An almost fully dense surface morphology can be seen in the HIPed composite (Fig. 4c), where isolated pores were practically absent, indicating a higher density as result of pore removal during hot isostatic pressing treatments.

When multi-wall carbon nanotubes reinforced zirconia toughened alumina nanocomposites are carefully manufactured and

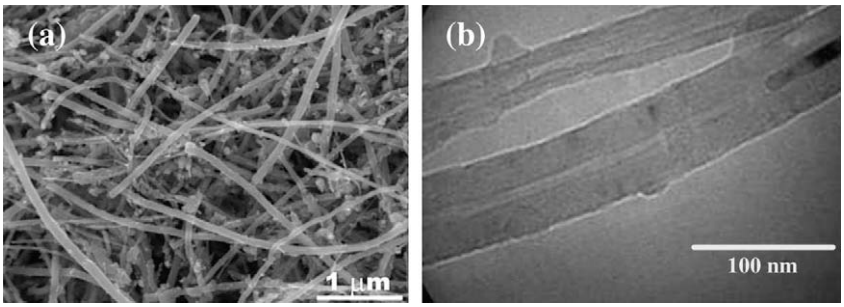

Fig. 2. Typical SEM (a) and TEM (b) micrographs of the starting MWCNT synthesized by spray pyrolysis.

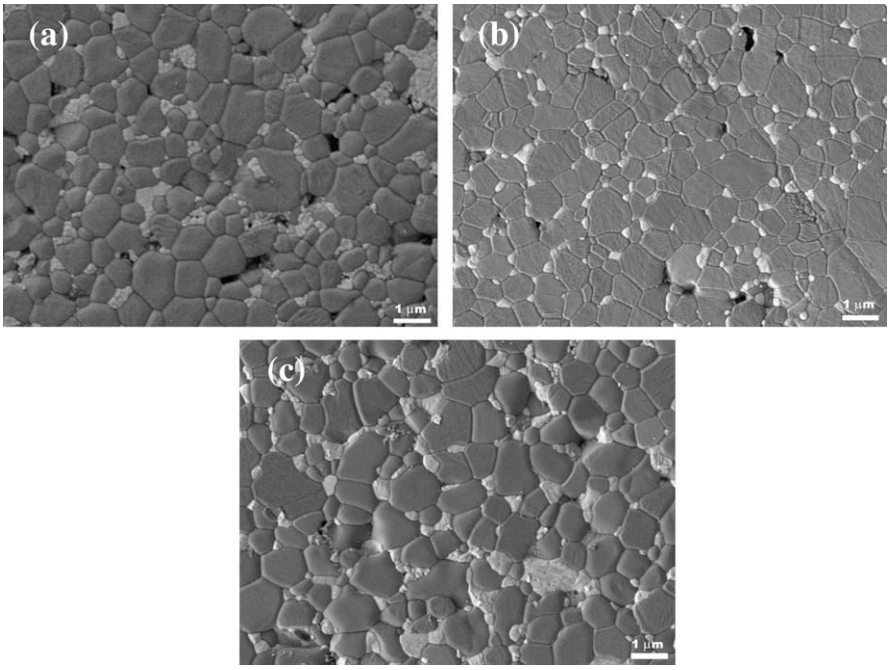

Fig. 4. Typical SEM micrographs of polished and thermally etched surfaces of as-pressureless sintered Al_2O_3 + 0.025% MgO + 13% TZ-3Y + 2% $ZrO_{2(m)}$ composite with additions of (a) 0.01 wt.%, (b) 0 wt.% of MWCNT, and (c) pressureless sintered and HIPed composite with 0.01 wt.% of MWCNT.

the optimization of powder processing is possible, the obtained Vickers hardness values are higher than 14 GPa. The dependence of Vickers hardness and grain size on carbon nanotubes content in the pressureless sintered composite before and after HIP treatment is illustrated in Fig 5a and b, respectively. From this figure it is clearly observed that for a constant amount of carbon nanotubes additions, the hardness is increased when hot isostatic pressing is applied to the composites, related to their higher relative density. Regarding the influence of the CNT content, it can be seen that for pressureless sintered samples the hardness decreases when the carbon nanotubes content is increased (Fig. 5a). On the other hand, in HIPed samples a decreased in hardness is observed for contents of 0.005 wt.% CNTs, meanwhile a slightly increases in hardness is observed for additions of 0.01 wt.% of carbon nanotubes (Fig. 5b), although its hardness is also lower than the composite without CNTs additions. On the other side, it is observed that Vickers hardness for pressureless sintered and HIPed samples decreased with final grain size up to 0.005 wt.% of carbon nanotubes additions indicating a major residual porosity in the case of pressureless sintered specimens (Fig. 3), which in turn could inhibit the grain boundary migration during sintering process hindering the grain growth. For contents of 0.01 wt.% CNTs, the hardness had a slight increasing when the grain size is also increased due to the reduction of remain porosity facilitating the grain boundary migration resulting in a slight grain growth [29].

It is known that the hardness of ceramic materials is usually affected by the intrinsic deformability of the ceramic and different microstructural parameters such as multiphases, grain size and orientation, porosity [30]. In the existing literature, the hardness and the fracture toughness values of ceramics are commonly reported as a function of the grain size. For example, Daguano et al. [31] reported reduction on hardness in sintered ZrO_2–Al_2O_3 attributed to increase of the grain size. Suzuki et al. [32] reported that Vickers hardness is correlated with porosity and grain size. Whereas, no significant dependence of Vickers microhardness on grain size was reported by Chaim and Hefetz [33] in nanocrystalline ZrO_2–3 wt.% Y_2O_3 cold pressed, presintered and hot isostatic pressing (HIP) to dense specimens, a direct influence of remain porosity on the hardness was reported by Jiang et al. [34] in Al_2O_3–10 vol.% SWCNTs composite sintered by SPS at different temperatures.

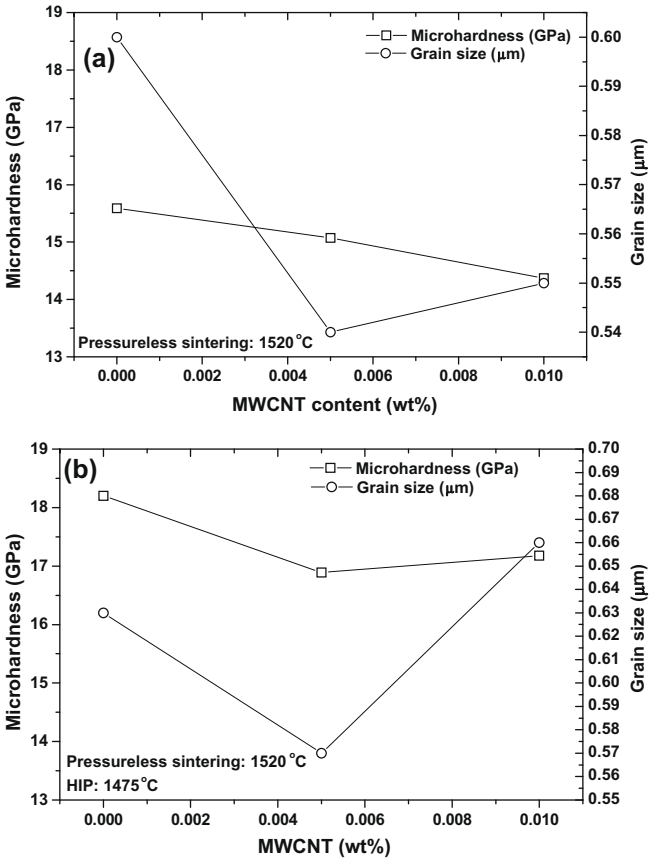

Fig. 5. Dependence of Vickers hardness and grain size on MWCNT content in the Al_2O_3 + 0.025% MgO + 13% TZ-3Y + 2% $ZrO_{2(m)}$ composite pressureless sintered (a), and after HIP treatment (b).

Fig. 6 shows the dependence of fracture toughness and grain size on carbon nanotubes content in the pressureless sintered composite before (Fig. 6a) and after (Fig. 6b) hot isostatic pressing treatment. It can be seen that for the "as sintered" samples (Fig. 6a) the fracture toughness increases with the addition of carbon nanotubes, while the grain size decreases at contents of 0.005 wt.% MWCNTs remaining constant at contents of 0.01 wt.%. Conversely, in HIPed samples a slight increase in grain size is observed at 0.01 wt.% MWCNTs content which would be in disagreement with experiments reported by Zhan et al. [24] where the results suggested that carbon nanotubes could inhibit the grain growth in ceramic matrix composites. After HIP treatment (Fig. 6b) it can be seen that with 0.005 wt.% MWCNTs additions, the fracture toughness of the sintered nanocomposites is lower than that obtained for the nanocomposite free of carbon nanotubes, whereas for 0.010 wt.% MWCNT the fracture toughness increases, indicating that the mechanical properties could be enhanced only if an optimum amount of carbon nanotubes are present in the matrix of the composite. Therefore, this low fracture toughness in 0.005 wt.% carbon nanotubes content could be due to poor bonding of CNTs to the matrix (for the presence of many pores in the composite so they did not carry the load which must be distributed throughout the nanotube in order to ensure that the outermost layer did not shear off [18]).

As can be seen from Fig. 6b, the composite with 0.01 wt.% CNTs addition possess the higher fracture toughness (~4.4 MPa $m^{1/2}$) being about 7% and 37% higher than that of the sample without HIP treatment (~4.1 ± 0.78 MPa $m^{1/2}$) and "as sintered" (3.2 ± 0.5 MPa $m^{1/2}$, Fig. 6a) composite without additions of carbon nanotubes, respectively. On the other side, an increasing in grain size in HIPed composites was observed for the different contents of CNTs compared with samples without hot isostatic pressing treatment. This behavior could be related to the pore removal during HIP and this can be supported in Fig. 3 where an increase in relative density after HIP treatment denotes an additional shrinkage as consequence of the removal of closed porosity. Note in this figure that the lower relative density corresponded at pressureless sintered composites with additions of 0.005 wt.% carbon nanotubes and where the pore removal was remarkable, and reached the higher relative density after hot isostatic pressing (~98%). In contrast, it can be noticed that an addition of 0.005 wt.% of carbon nanotubes to the composite produces a decrease of grain size, both before and after HIP, whereas higher additions (0.01 wt.% MWCNTs) slightly increase grain size (more significantly by HIP). The intimate contact between carbon nanotubes and matrix suggests that the extent of interfacial bonding will be a factor in increasing the toughness in HIPed samples, and not grain size, with additions of 0.01 wt.% MWCNT nanocomposites. Conversely, in HIPed samples with additions of 0.005 wt.% carbon nanotubes, the network structure seem to disappear and the fracture toughness is slightly lowered [24]. We could speculate that the amount of carbon nanotubes was not enough to obtain a homogeneous dispersion in the whole ceramic matrix, thus weak regions were originated where the cracks could nucleate, leading thus to the decreasing of hardness and fracture toughness. For a better understanding, Table 1 summarizes the mechanical properties of "as pressureless" sintered composites and HIPed ones at 1475 °C (diagrams Figs. 3, 5 and 6) as a function of multi-wall carbon nanotubes (MWCNTs) content.

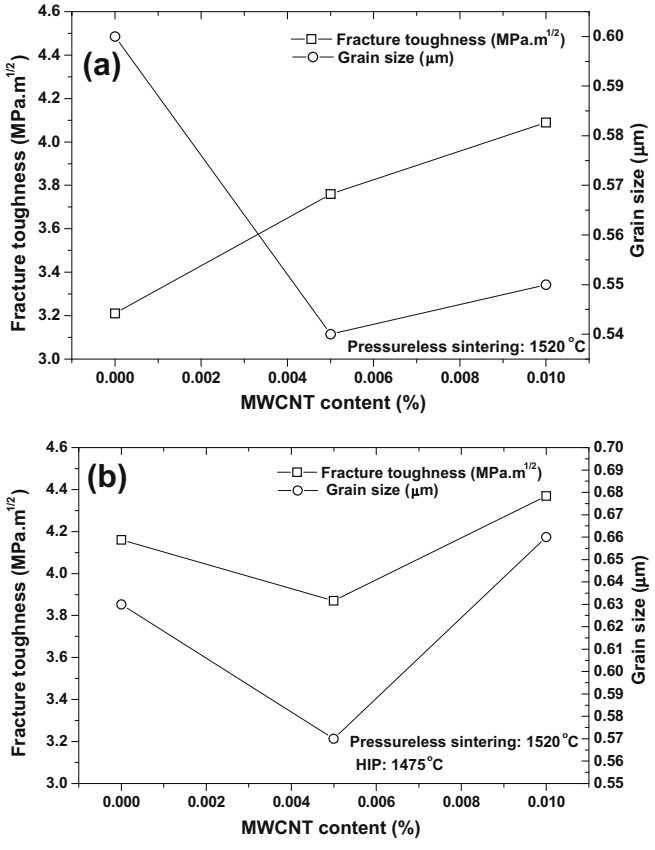

Fig. 6. Dependence of the fracture toughness and grain size on MWCNT content in the Al_2O_3 + 0.025% MgO + 13% TZ-3Y + 2% $ZrO_{2(m)}$ composite pressureless sintered (a), and after HIP treatment (b).

Fig. 7 shows a representative SEM micrograph of typical Vickers hardness impressions obtained on the polished and thermally etched surface in the "as sintered" without additions (a), with additions of 0.01 wt.% MWCNTs (b), and sintered and HIPed with additions (c) of 0.01 wt.% MWCNTs Al_2O_3 + 0.025% MgO + 13% TZ-3Y + 2% $ZrO_{2(m)}$ ceramic nanocomposites. The cracks emanating from the four vertices were measured to determine K_{IC}. From this figure it is observed that the size of the indent in the HIPed composite (Fig. 7c) is slightly smaller that the indent corresponding to the "as sintered" samples (Fig. 7a and b without and with additions of 0.01 wt.% MWCNT, respectively). This suggests a smaller intrinsic deformability of the HIPed composites as consequence of a lower percentage of final porosity. The figures clearly demonstrate the well-developed and almost symmetrical radial-median crack morphology and that multiple cracking from single indent corner is absent. At the applied load the plastic deformation could be predominant and as a result much of the indentation energy is consumed for material flow and displacement, which lowers the apparent hardness in "as sintered" without HIP with additions of 0.01 wt.% MWCNTs (Fig. 7a and b).

On the other hand, observations at higher magnification of one arm of an indented "as sintered" without additions (Fig. 7d), with additions of 0.01 wt.% MWCNTs (Fig. 7e), and sintered and HIPed with additions of 0.01 wt.% MWCNT (Fig. 7f) ceramic nanocomposites marked as "1" in Fig. 7a–c, showed the evidence of crack deflection (zigzagged cracks). In Fig. 7d and e, the fracture pattern is almost exclusively intergranular with cracks occasionally propagating through the smaller grains. Similar appreciations have been reported by Correa de Sa e Benevides de Moraes et al. [35]. Fig. 7f corresponding to the HIPed composite with additions of 0.01 wt.% carbon nanotubes revealed a combined transgranular and intergranular fracture mode. On the other hand, the intragranular fracture mode indicates the grain boundary strengthening by the concurrent nanosized ZrO_2 particles added to the composite (see Fig. 7e and g). This behavior results in greater fracture energy which leads to greater fracture toughness [28,30]. Likewise, the toughening mechanism in this nanocomposite can be explained

Table 1
Summary of mechanical properties of "as pressureless" sintered samples and HIPed ones at 1475 °C as a function of multi-wall carbon nanotubes (MWCNTs) content.

MWCNTs (wt.%)	Pressureless sintering at 1520 °C				Pressureless sintering at 1520 °C and HIP at 1475 °C			
	Relative density (%)	Vickers hardness (GPa)	Fracture toughness (MPa $m^{1/2}$)	Grain size (μm)	Relative density (%)	Vickers hardness (GPa)	Fracture toughness (MPa $m^{1/2}$)	Grain size (μm)
0	95.61	15.59 ± 2.1	3.21 ± 0.5	0.60 ± 0.2	97.45	18.20 ± 0.9	4.2 ± 0.8	0.63 ± 0.2
0.005	94.38	15.07 ± 1.2	3.76 ± 0.5	0.54 ± 0.2	97.70	16.89 ± 1.6	3.9 ± 0.7	0.57 ± 0.2
0.01	95.11	14.37 ± 1.3	4.09 ± 0.5	0.55 ± 0.2	97.60	17.18 ± 1.1	4.4 ± 0.6	0.66 ± 0.3

by a crack bridging effect of the multi-wall carbon nanotubes shown in Fig. 7g and labeled as a circle, where the carbon nanotube bridge the two crack surfaces and remain intact during the crack propagation.

Additional to the mentioned toughening mechanism, pulled-out carbon nanotubes was also observed on the fracture surface of the HIPed nanocomposite with additions of 0.01 wt.% MWCNT, as can be seen in Fig. 8a and b (indicated by arrow marks). It is clearly observed that the interface between CNTs and Al_2O_3 matrix is strongly bonded conducing to a significant load transfer from the matrix to the carbon nanotubes during loading. It is noteworthy in the microstructure that some carbon nanotubes were entangled with Al_2O_3 grains. Similar observations have been reported by Mo et al. [17] in carbon nanotubes reinforced alumina matrix nanocomposite prepared by sol–gel process and Ahmad and Pan [28] with hybrid nanocomposites based alumina.

From an analysis of the crack geometry for each tested composite (Fig. 7d–f) it is possible to assume that the tortuosity of the crack path tend to follow the grain boundaries (Fig. 7d and e) and then, the crack deflection mechanism takes place and gives a crack profile corresponding to the sample microstructure. The deflection mechanism (less effective) [36] accompanied by the presence of transgranular fracture as can be seen in Fig. 7f, leads to a relatively high fracture toughness value. It is believed [37] that the presence of a low degree of crack deflection depends on the grain shape and on the intergranular fracture mechanism.

Taking into account the different thermal expansion coefficient of the Al_2O_3 ($5.5–8.1 \times 10^{-6}\ °C^{-1}$) matrix, ZrO_2 (TZ-3Y) ($10.3 \times 10^{-6}\ °C^{-1}$) grains, monoclinic ZrO_2 ($6.5 \times 10^{-6}\ °C^{-1}$) nanosized particles, and MWCNTs ($1.6–2.6 \times 10^{-5}\ °C^{-1}$), it is speculated [38] that an additional increase in fracture toughness in the HIPed Al_2O_3 + 0.025% MgO + 13% TZ-3Y + 2% $ZrO_{2(m)}$ nanocomposite with

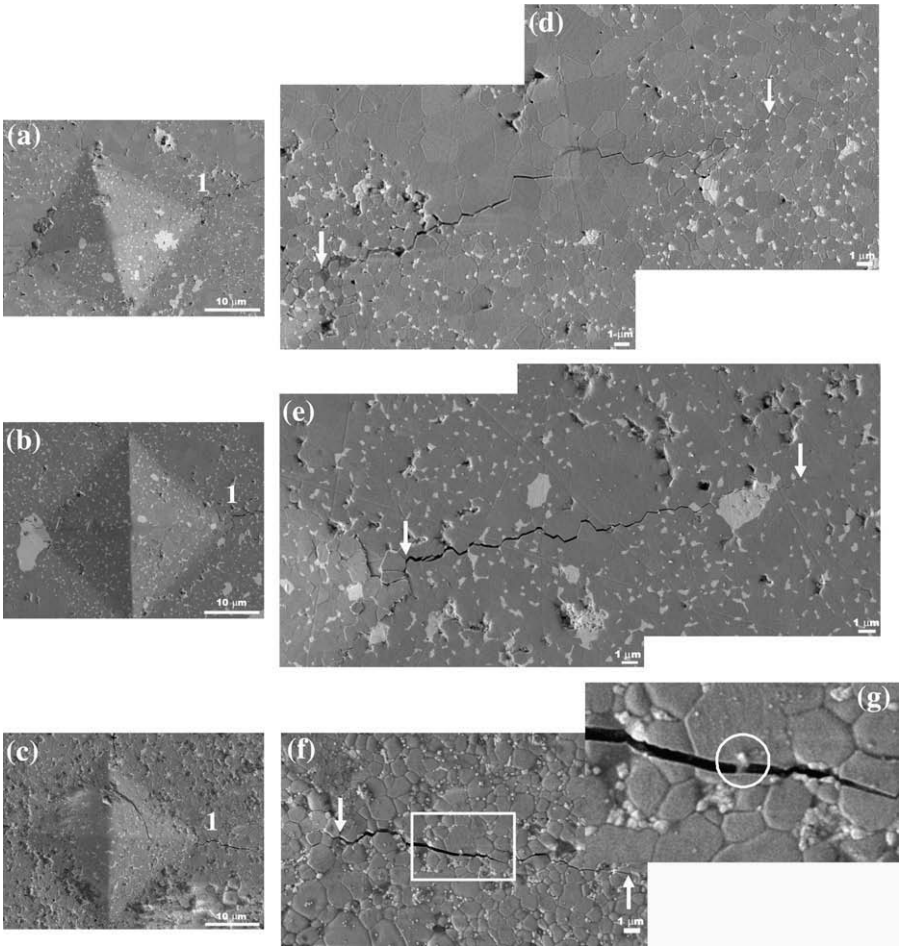

Fig. 7. SEM of typical hardness impressions in Al_2O_3 + 0.025% MgO + 13% TZ-3Y + 2% $ZrO_{2(m)}$ composites. "As sintered" without (a) and with additions (b) 0.01 wt.% MWCNT, and sintered and HIPed with additions of 0.01 wt.% MWCNT (c). Magnification of the arm cracks labeled as "1" in (a–c) are shown in (d–f). Square indicated in (f) is closed up in (g). The arrow marks indicate the beginning and final of the crack. Circle is explained in text. Bars correspond to 10 and 1 μm in (a–c) and (d–f), respectively.

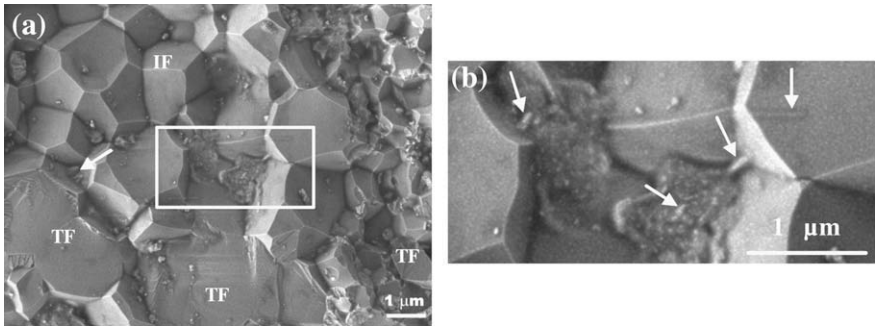

Fig. 8. SEM of fracture surface of the pressureless sintered and HIPed Al_2O_3 + 0.025% MgO + 13% TZ-3Y + 2% $ZrO_{2(m)}$ composite with additions of 0.01 wt.% MWCNT (a); magnification corresponding to square in (a) is shown in (b). IF = intergranular fracture, TF = transgranular fracture. Arrow marks in (a and b) are explained in text.

additions of 0.01 wt.% MWCNT ceramic nanocomposite could be due to the increase in the amount of transformed monoclinic phase on the fracture surface of the specimen, as result from the induced stresses owing to mismatch between thermal expansion coefficient of the alumina matrix and the CNTs used as reinforcement [10,28].

4. Conclusions

From the investigated multi-wall carbon nanotubes reinforced $Al_2O_{3(n)}/MgO_{(n)}/ZrO_2(TZ\text{-}3Y)_{(n)}/ZrO_{2(n)m}$ (m = monoclinic) nanocomposite pressureless sintered and sinter + HIPed, we can conclude:

(1) By using an adequate anti-oxidation sagger and a graphite powder bed, it is possible to sinter in air MWCNTs reinforced zirconia toughened alumina (ZTA), with concurrent reinforcement of 2 wt.% monoclinic nanosized ZrO_2.
(2) Relative densities above 94% were attained by pressureless sintering with and without additions of multi-wall carbon nanotubes (MWCNTs). The subsequent application of the hot isostatic pressing treatment leads for all composites to an increase of their relative density. In all cases the grain size was maintained at submicron scale at the processing temperatures. Grain sizes between 0.46 ± 0.20 and 0.53 ± 0.20 μm and 0.49 ± 0.20 and 0.6 ± 0.3 μm were obtained for pressureless sintered composites before and after HIP, respectively.
(3) The Vickers hardness values decreased with the addition of MWCNTs in both pressureless sintered and HIPed samples. However, for the same amount of MWCNTs the hardness increases with hot isostatic pressing treatment; in composites with additions of 0.01 wt.% MWCNTs the hardness can be increased up to ~19%.
(4) The fracture toughness values were increased with the carbon nanotubes content for pressureless sintered composite. Meanwhile, for HIPed composites a slight decreasing in fracture toughness was attained with the addition of 0.005 wt.% of MWCNTs. When hot isostatic pressing is applied, it is possible to obtain an increase in fracture toughness of ~7% and ~36% compared to the "as sintered" composites with 0.01 wt.% CNTs and free of carbon nanotubes, respectively.
(5) A combined transgranular and intergranular fracture mode was observed in HIPed composite with additions of 0.01 wt.% MWCNTs. The intragranular fracture mode indicates the grain boundary strengthening by the concurrent nanosized ZrO_2 particles added to the composite. This behavior results in greater fracture energy which leads to greater fracture toughness. Crack deflection and change of fracture mode from transgranular to intergranular, pull-outs of a small amount of carbon nanotubes, the bridging effect of CNTs during crack propagation, as well as thermal expansion mismatch between the alumina matrix and CNTs are the possible mechanisms that lead to the improvement in fracture toughness.
(6) The presence of some carbon nanotubes agglomerates indicates that there are difficulties in the preparation of defect-free MWCNTs reinforced ZTA nanocomposites and therefore, the mixing procedure needs to be improved. The presence of such agglomerates could be responsible for the lower density of the 0.005 wt.% MWCNTs content composite.
(7) The values reported in this work for zirconia toughened alumina nanocomposite reinforced with multi-wall carbon nanotubes and nanosized ZrO_2 particles would offer an alternative for the development in the field of orthopedic implants although there are still great challenges to the obtaining of well-dispersed carbon nanotubes–ceramic composites.

Acknowledgements

The authors wish to express their appreciation to W. Antunez for the SEM characterization and A. Nevarez-Rascón for hardness and fracture toughness measurements.

References

[1] An JW, Lim D-S. Effect of carbon nanotube additions on the microstructure of hot-pressed alumina. J Ceram Proc Res 2002;3(3):201–4.
[2] Duszova A, Dusza J, Tomasek K, Blugan G, Kuebler J. Microstructure and properties of carbon nanotube/zirconia composite. J Eur Ceram Soc 2008;28:1023–7.
[3] Hirvonen A, Nowak R, Yamamoto Y, Sekino T, Niihara K. Fabrication, structure, mechanical and thermal properties of zirconia-based ceramic nanocomposites. J Eur Ceram Soc 2006;26:1497–505.
[4] Iijima S. Helical microtubules of graphitic carbon. Nature 1991;354:56–8.
[5] Thostenson ET, Ren Z, Chou T-W. Advances in the science and technology of carbon nanotubes and their composites: a review. Compd Sci Technol 2001;61:1899–912.
[6] Chang S, Doremus RH, Siegel RW, Ajayan PM. Ceramic matrix nanocomposites containing carbon nanotubes for enhanced mechanical behavior. Patent No. US 6,420,293 B1; 2002.
[7] Sun J, Gao L, Jin X. Reinforcement of alumina matrix with-multiwalled carbon nanotubes. Ceram Int 2005;31:893–6.
[8] Ebbesen TW. In: Carbon nanotubes: preparation and properties. CRC Press; 1997. p. 277.
[9] Yu MF, Lourie O, Dyer MJ, Moloni K, Kelly TF, Ruoff RS. Strength and breaking mechanism of multiwalled carbon nanotubes under tensile load. Science (Washington, DC) 2000;287:637–40.
[10] Zhan G-D, Mukherjee AK. Carbon nanotube reinforced alumina-based ceramics with novel mechanical, electrical, and thermal properties. Int J Appl Ceram Technol 2004;1(2):161–71.

[11] Lupo F, Kamalakaran R, Scheu C, Grobert N, Ruhle M. Microstructural investigations on zirconium oxide–carbon nanotube composites synthesized by hydrothermal crystallization. Carbon 2004;42:1995–9.
[12] Peigney A, Laurent Ch, Flahaut E, Rousset A. Carbon nanotubes in novel ceramic matrix nanocomposites. Ceram Int 2000;26:677–83.
[13] Samal SS, Bal S. Carbon nanotube reinforced ceramic matrix composites – a review. J Miner Mater Char Eng 2008;7(4):355–70.
[14] Aguilar EA, Antunez W, Alonso G, Paraguay F, Espinosa F, Miki-Yoshida M. Study of carbon nanotubes síntesis by spray pyrolysis and model of growth. Diamond Rel Mater 2006;15:1329–35.
[15] Sun J, Iwasa M, Nakayama T, Niihara K, Gao L, Jin X. Pressureless sintering of alumina carbon nanotubes composites in air atmosphere furnace and their mechanical properties. J Ceram Soc Jpn 2004;112(5 Suppl. 112-1):S403–6 [PacRim5 special issue].
[16] Fan J, Zhao D, Wu M, Xu Z, Song J. Preparation and microstructure of multi-wall carbon nanotubes–toughened Al_2O_3 composite. J Am Ceram Soc 2006;89(2):750–3.
[17] Mo ChB, Cha SI, Kim KT, Lee KH, Hong SH. Fabrication of carbon nanotube reinforced alumina matrix nanocomposite by sol–gel process. Mater Sci Eng 2005;A395:124–8.
[18] Zhu Y-F, Shi L, Liang J, Hui D, Lau K-T. Synthesis of zirconia nanoparticles on carbon nanotubes and their potential for enhancing the fracture toughness of alumina ceramics. Composites B 2008;39:1136–41.
[19] Zhang F-J, Yang L, Huang X-Y, Zhu De-G. The character of sintering under vacuum and its use in hot isostatic pressing in comparison with the air pre-sintering and slurry coating techniques for alumina–zirconia composites. J Mater Process Technol 1998;74:115–21.
[20] Sun J, Gao L, Iwasa M, Nakayama T, Niihara K. Failure investigation of carbon nanotube/3Y-TZP nanocomposites. Ceram Int 2005;31:1131–4.
[21] Zhan GD, Kuntz JD, Garay JE, Murkherjee AK, Zhu P, Koumoto K. Thermoelectric properties of carbon nanotube/ceramic nanocomposites. Scr Mater 2006;54:77–82.
[22] An JW, You DH, Lim DS. Tribological properties of hot-pressed alumina–CNT composites. Wear 2003;255:677–81.
[23] Siegel RW, Chang SK, Ash BJ, Stone J, Ajayan PM, Doremus RW, et al. Mechanical behavior of polymer and ceramic matrix nanocomposites. Scr Mater 2001;44:2061–4.
[24] Zhan GD, Kuntz JD, Wan J, Mukherjee AK. Single-wall carbon nanotubes as attractive toughening agents in alumina based nanocomposites. Nature 2002;2:38–42.
[25] Santos C, Maeda LD, Cairo CAA, Acchar W. Mechanical properties of hot-pressed ZrO_2–NbC ceramic composites. Int J Ref Met Hard Mater 2008;26:14–8.
[26] Spear RL, Cameron RE. Carbon nanotubes for orthopaedic implants. Int J Mater Form 2008;1:127–33.
[27] Evans AG, Charles EA. Fracture toughness determinations by indentation. J Am Ceram Soc 1976;59:371–2.
[28] Ahmad K, Pan W. Hybrid nanocomposites: a new route towards tougher alumina ceramics. Compd Sci Technol 2008;68:1321–7.
[29] Peigney A, Flahaut E, Laurent Ch, Chastel F, Rousset A. Aligned carbon nanotubes in ceramic-matrix nanocomposites prepared by high-temperature extrusion.. Chem Phys Lett 2002;352:20–5.
[30] Tekeli S. Fracture toughness (K_{IC}), hardness, sintering and grain growth behaviour of 8YSCZ/Al_2O_3 composites produced by colloidal processing. J Alloys Compd 2005;391:217–24.
[31] Daguano JKMF, Santos C, Souza RC, Balestra RM, Strecker K, Elias CN. Properties of ZrO_2–Al_2O_3 composite as a function of isothermal holding time. Int J Ref Met Hard Mater 2007;25:374–9.
[32] Suzuki HY, Shinosaki K, Kuroi H, Tashima S. Sintered microstructure and mechanical properties of high purity alumina ceramics made by high-speed centrifugal compaction process. Key Eng Mater 1999;159–160:187–92.
[33] Chaim R, Hefetz M. Effect of grain size on elastic modulus and hardness of nanocrystalline ZrO_2–3 wt% Y_2O_3. J Mater Sci 2004;39:3057–61.
[34] Jiang D, Thomson K, Kuntz JD, Ager JW, Mukherjee AK. Effect of sintering on a single-wall carbon nanotube–toughened alumina-based nanocomposites. Scr Mater 2007;56:95962.
[35] Correa de Sa e Benevides de Moraes MC, Elias CN, Filho JD, Guimaraes de Oliveira L. Mechanical properties of alumina–zirconia composites for ceramic abutments. Mater Res 2004;7:634–49.
[36] Celli A, Tucci A, Esposito L, Palmonari C. Fractal analysis of crack in alumina–zirconia composites. J Eur Ceram Soc 2003;23:469–79.
[37] Celli A, Tucci A, Esposito L. Quantitative evaluation by fractal analysis of indentation crack paths in Si_3N_4–SiC_w composites. J Eur Ceram Soc 1999;19:441–9.
[38] Roberts JM, Singh JP, Scattergood RO. Microstructure and properties of alumina–whisker-reinforced tetragonal polycrystal matrix composites. CONF-910162-1; 1991.